

Study of the thermochromic phase transition in
CuMo_{1-x}W_xO₄ solid solutions at the W L₃-edge by
resonant X-ray emission spectroscopy

Inga Pudza^{a,*}, Aleksandr Kalinko^{a,b}, Arturs Cintins^a, Alexei Kuzmin^{a,**}

^a*Institute of Solid State Physics, University of Latvia, Kengaraga street 8, LV-1063 Riga, Latvia*

^b*Department of Chemistry and Center for Sustainable Systems Design, Paderborn University, 33098 Paderborn, Germany*

Abstract

Polycrystalline CuMo_{1-x}W_xO₄ solid solutions were studied by resonant X-ray emission spectroscopy (RXES) at the W L₃-edge to follow a variation of the tungsten local atomic and electronic structures across thermochromic phase transition as a function of sample composition and temperature. The experimental results were interpreted using ab initio calculations. The crystal-field splitting parameter Δ for the 5d(W)-states was obtained from the analysis of the RXES plane and was used to evaluate the coordination of tungsten atoms. Temperature-dependent RXES measurements were successfully employed to determine the hysteretic behaviour of the structural phase transition between the α and γ phases in CuMo_{1-x}W_xO₄ solid solutions on cooling and heating, even at low ($x < 0.10$) tungsten content. It was found that tungsten ions

*Corresponding author

**Corresponding author

Email addresses: inga.pudza@cfi.lu.lv (Inga Pudza),
aleksandr.kalinko@desy.de (Aleksandr Kalinko), arturs.cintins@cfi.lu.lv
(Arturs Cintins), a.kuzmin@cfi.lu.lv (Alexei Kuzmin)

have octahedral coordination for $x > 0.15$ in the whole studied temperature range (90-420 K), whereas their coordination changes from tetrahedral to octahedral upon cooling for smaller ($x \leq 0.15$) tungsten content. Nevertheless, some amount of tungsten ions was found to co-exists in the octahedral environment at room temperature for $x < 0.15$. The obtained results correlate well with the color change in these solid solutions.

Keywords: $\text{CuMo}_{1-x}\text{W}_x\text{O}_4$, crystal-field splitting, resonant X-ray emission spectroscopy (RXES), high-energy resolution fluorescence detected X-ray absorption near-edge structure (HERFD-XANES)

1. Introduction

$\text{CuMo}_{1-x}\text{W}_x\text{O}_4$ solid solutions represent a class of functional materials demonstrating a wide range of physical and chemical properties such as thermochromic [1, 2, 3, 4, 5, 6], piezochromic [2, 5, 7], halochromic [8], photoelectrochemical [9], thermosensitive [5] and catalytic [10].

The strongest thermochromic effect is observed on cooling for small tungsten content ($x < 0.15$), when the change of the material color from green to brown is due to the first-order phase transition caused by the Mo(W) displacement from the tetrahedral site (as in $\alpha\text{-CuMoO}_4$) to the octahedral site (as in $\gamma\text{-CuMoO}_4$) (Fig. 1) [1, 5, 11]. The similar color change occurs also in $\alpha\text{-CuMoO}_4$ on heating [12], however, in this case, no phase transition takes place, the coordination of metal ions remains unchanged, and the variation of color is due to the lattice expansion and strong enhancement of specific thermal disorder [13]. For tungsten content above $x \sim 0.15$, $\text{CuMo}_{1-x}\text{W}_x\text{O}_4$ solid solutions crystallize in the wolframite-type structure with the octahedral coordination of metal ions and do not manifest pronounced thermochromic behaviour. Therefore, the knowledge of the local environment of metal ions in these mixed compounds is crucial for understanding and controlling their properties.

Conventionally, X-ray absorption spectroscopy (XAS) is used to probe the local environment of atoms in complex materials [14, 15, 16]. However, in the case of tungstates and molybdates, often composed from strongly distorted polyhedra, the recovery of structural information from XAS requires the use of a computationally heavy and time-consuming approach based on reverse Monte Carlo (RMC) simulations [17, 18, 19, 20]. Moreover, we have

previously shown that a reliable structural analysis requires the knowledge of X-ray absorption spectra at least for all metal edges [17, 21]. In the case of solid solutions, the low content of one of the component limits the quality of the experimental data, which additionally complicates the analysis. Finally, the close values of the metal–oxygen interatomic distances in the radial distribution functions (RDFs) obtained using the RMC simulation make it often difficult to unambiguously identify the atoms belonging to the first coordination shell of metal and, as a result, the type of its coordination polyhedron.

In tungsten oxides and related materials, the splitting of the tungsten 5d band depends on the crystal field of ligands and can be experimentally probed by the W L₃-edge XAS [22, 23], that can be used to distinguish between different local symmetries of the tungsten coordination polyhedron. In particular, the tungsten 5d-band splits into 5d(*t*_{2g}) and 5d(*e*_g) sub-bands in octahedral and 5d(*t*₂) and 5d(*e*) sub-bands in tetrahedral coordination. However, the small value of the crystal field splitting (about several electron volts) and the large value of the natural width of the excited 2p_{3/2}(W) level (~ 4.5 eV [24]) often mask the difference between the two coordinations [25, 26, 27]. Therefore, a more sophisticated experimental approach should be used to more reliably address this issue.

In this study, we used the resonant X-ray emission spectroscopy (RXES) at the W L₃-edge to determine a variation of the tungsten local atomic and electronic structure in CuMo_{1-x}W_xO₄ solid solutions across thermochromic phase transition as a function of sample composition and temperature. We demonstrate that the analysis of the W L₃-edge white line splitting provides

a robust tool for distinguishing tetrahedral and octahedral coordinations of tungsten ions in these solid solutions.

2. Experimental details

Polycrystalline $\text{CuMo}_{1-x}\text{W}_x\text{O}_4$ powders were synthesized using a solid-state reaction method by heating a mixture of CuO and MoO_3 powders with a stoichiometric amount of WO_3 at 650°C in air for 8 hours followed by cooling down to the room temperature. One group of samples with $x \leq 0.15$ was greenish, and the second group with $x \geq 0.20$ was brownish. All samples were characterized by X-ray powder diffraction and micro-Raman spectroscopy (see in the Supplementary Information).

The temperature-dependent RXES experiments were performed at the P64 Advanced X-Ray Absorption Spectroscopy beamline of the PETRA III (HASYLAB/DESY) storage ring using recently constructed RXES endstation [28, 29]. The X-ray beam from an undulator was monochromatized by a liquid-nitrogen-cooled double-crystal $\text{Si}(311)$ monochromator and focused in vertical and horizontal planes ($100 \mu\text{m} \times 240 \mu\text{m}$) by two mirrors with Rh coating positioned downstream of the monochromator. The high stability and high intensity ($5 \cdot 10^{11}$ photons/s) of the P64 beamline provided the possibility to accumulate high quality/resolution RXES data. The ionization chamber was used for incident X-ray intensity monitoring. The XES signal was dispersed by von Hamos-type spectrometer equipped with cylindrical bent $\text{Si}(444)$ analyser crystals [29] and collected by Dectris 2D Pilatus 300K detector. The monochromator was calibrated at the W L_3 -edge using tungsten foil and the energy scale of the spectrometer was set according to

the position of the elastic line on the detector. The inelastically scattered X-ray signal and W $L\alpha_1$ and $L\alpha_2$ fluorescence were acquired in the RXES plane. The high-resolution W L_3 -edge XANES (HERFD-XANES) was extracted from the RXES plane at fixed emission energy 8398.5 ± 0.2 eV. The temperature of the sample was controlled using liquid nitrogen (LN_2) cryostat Linkam THMS600 in the range of 90-450 K. All samples were measured in the form of sintered powders.

The W L_3 -edge XANES spectra of the same powder samples recorded at room-temperature in transmission mode at the Elettra XAFS bending-magnet beamline [30] were used for comparison. The experimental details can be found in [13].

3. FDMNES calculations

The simulation of the experimental W L_3 -edge XANES spectra was performed based on the finite difference method (FDM) by the ab initio real-space FDMNES code [31, 32], thus avoiding the muffin-tin potential approximation. The XANES spectra were calculated using real energy-dependent Hedin-Lundqvist exchange-correlation potential [33] taking into account spin-orbit interactions and the self-consistent cluster potential. The calculations were performed for 4.0 Å radius clusters constructed around the absorbing tungsten atom from the crystallographic structures of interest, since the effect of the crystal field is related to the interaction between tungsten and nearest oxygen atoms.

All calculated XANES spectra were convoluted with a Lorentzian broadening function with a FWHM given by $\Gamma_{hole}=1$ eV to mimic the broadening

due to the core-hole lifetime and experimental resolution. The effect of the core-hole was also examined by performing calculations for the excited (with the core hole) and non-excited (without the core hole) absorbing tungsten atom.

The structures of α -CuMoO₄ and γ -CuMoO₄ contain three non-equivalent sites for copper (Cu1, Cu2, Cu3) and molybdenum (Mo1, Mo2, Mo3) atoms [34]. However, all molybdenum atoms occupy either distorted tetrahedral (in α -CuMoO₄) or distorted octahedral (in γ -CuMoO₄) positions. In CuWO₄, there is only one tungsten position with distorted octahedral coordination [35].

The calculated W L₃-edge XANES spectra are shown in Fig. 2 for CuWO₄ and tungsten atom substituting molybdenum atom at the Mo2 site in α -CuMoO₄ (distorted tetrahedral environment) and γ -CuMoO₄ (distorted octahedral environment). The XANES spectra calculated for tungsten atoms placed at the Mo1 or Mo3 sites are close to that at the Mo2 site and are not shown. Note that all calculations were performed based on the crystallographic structures obtained from diffraction [34, 35], without any structure relaxation due to the substitution.

4. Results and discussion

4.1. Crystal field splitting in the W L₃-edge XANES & RXES

At ambient conditions, CuMo_{1-x}W_xO₄ solid solutions exist in one of three crystal structures with triclinic $P\bar{1}$ symmetry, which are isostructural to the high-pressure phases of CuMoO₄ [34]. In the α -phase, 2/3 and 1/3 of Cu²⁺ cations form distorted CuO₆ octahedra and CuO₅ square-pyramids, respec-

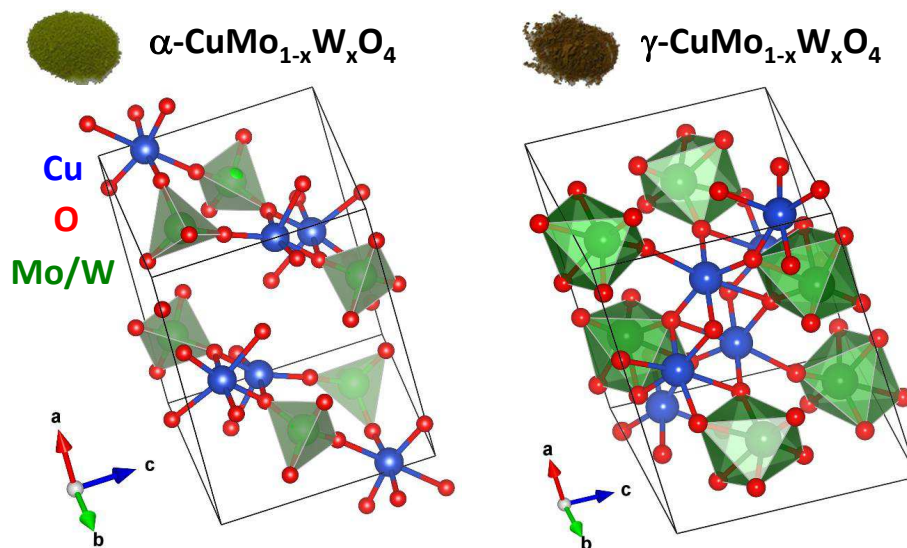


Figure 1: Crystal structures and unit cells of high-temperature green (α) and low-temperature brownish-red (γ) $\text{CuMo}_{1-x}\text{W}_x\text{O}_4$ phases [5, 34]. MoO_4 and MoO_6 polyhedra are indicated in the α - and γ -phases, respectively. Small red balls are oxygen atoms, medium-sized blue balls are copper atoms, and large green balls are molybdenum/tungsten atoms. Photographs of the two phases are also shown.

tively, whereas Mo^{6+} cations form MoO_4 tetrahedra. The crystal structure of $\gamma\text{-CuMoO}_4$ is built up of distorted CuO_6 and MoO_6 octahedra. Finally, $\text{CuMoO}_4\text{-III}$ phase has a wolframite-type structure, in which both Cu^{2+} and Mo^{6+} ions occupy octahedral sites. The sequence ($\alpha \rightarrow \gamma \rightarrow \text{III}$) of structural transitions upon increasing W content is similar to that under hydrostatic pressure [34]. Therefore, the ability to tune the functional properties of $\text{CuMo}_{1-x}\text{W}_x\text{O}_4$ solid solutions by the introduction of tungsten ions is often explained by the effect of locally-induced chemical pressure that appears due to a small difference between the ionic radii of Mo^{6+} (0.59 Å) and W^{6+} (0.60 Å) ions [36]. Besides, the increase of the $\alpha \leftrightarrow \gamma$ phase transition tem-

perature at high tungsten content was attributed to the stronger preference of tungsten ions to the octahedral environment [1, 2].

According to the crystal-field theory [37], the d-orbitals of the metal ion split in the octahedral field of six oxygen atoms into two groups (triply degenerate t_{2g} orbitals and doubly degenerate e_g orbitals) with the energy difference Δ_{oct} , where the t_{2g} orbitals have lower energy than the e_g ones. In tetrahedral coordination, the splitting of the d orbitals occurs into two groups with the energy difference Δ_{tet} between the lower energy, doubly degenerate e orbitals and the higher energy, triply degenerate t_2 orbitals. The splitting magnitudes for regular tetrahedral Δ_{tet} and octahedral Δ_{oct} coordinations are related as $\Delta_{tet} = 4/9\Delta_{oct}$ for similar W–O distances [37]. For oxidation state W^{6+} , all five d-orbitals are vacant, therefore, two electron transitions from $2p_{3/2}$ to split 5d states are possible and will have different X-ray absorption intensities. For tetrahedral WO_4 coordination, the intensity ratio will be $e:t_2=2:3$, whereas for octahedral WO_6 coordination, it will be $t_{2g}:e_g=3:2$. Thus, the knowledge of splitting value or intensity ratio for the two transitions in $CuMo_{1-x}W_xO_4$ solid solutions allows one to conclude on the type of tungsten ion coordination. Further, we will demonstrate how the analysis of the W L_3 -edge RXES data provides an opportunity to gain this information.

The XANES spectra of $CuMo_{1-x}W_xO_4$ solid solutions at the W L_3 -edge contain a strong resonance (see the inset in Fig. 2(a)), the so-called "white line" [38], located just below the continuum threshold and corresponding to the dipole-allowed electron transition from the $2p_{3/2}(W)$ level to a quasi-bound $5d(W)+2p(O)$ mixed-state in the presence of the core hole [25].

Although the W L_3 -edge XANES is sensitive to the coordination of the

absorbing atom, a very short natural lifetime of the excited state with the core hole at the $2p_{3/2}(W)$ level leads to significant intrinsic broadening (~ 4.5 eV [24]) of the absorption spectrum. As a result of the limited resolution, the crystal field splitting of the $5d(W)$ states is smeared out and cannot be usually resolved in the conventional transmission experiment (see the inset in Fig. 2(a)). However, some splitting of the white line maximum is nevertheless observed in the XANES spectrum measured in the transmission mode for a high tungsten content ($x = 0.75$).

Unlike the conventional XANES, RXES is a second-order process involving X-ray absorption and then X-ray emission described by the Kramers-Heisenberg formalism [39, 40, 41]. Experimental resolution is governed by the lifetime of intermediate and final states involved in the RXES process and Heisenberg's uncertainty principle. Note that the intermediate state of RXES is the same as the final state of the first-order optical process in XAS [42, 43, 44].

To interpret the experimental data, we performed the W L_3 -edge XANES calculations using the FDMNES code [31, 32]. As a result, information was obtained on the splitting of the $5d(W)$ orbitals for three local geometries of tungsten ions similar to those in $CuWO_4$, α - $CuMoO_4$ and γ - $CuMoO_4$ (Fig. 2). The white line in the calculated XANES spectra is split by about 4.0 eV and 3.0 eV, respectively, in $CuWO_4$ and γ - $CuMoO_4$ (W substitutes Mo at the Mo2 site) due to the distorted octahedral crystal-field, whereas a smaller splitting of about 2.0 eV is characteristic of a tungsten ion in the tetrahedral environment, as when it is located at the Mo2 site in α - $CuMoO_4$.

The splitting of the $5d(W)$ orbitals can be observed experimentally by

detecting the RXES due to $3d_{5/2}(\text{W}) \rightarrow 2p_{3/2}(\text{W})$ electron transition, since the lifetime of the final state with a hole at the $3d_{5/2}(\text{W})$ orbital is longer than that with a hole at the $2p_{3/2}(\text{W})$ orbital (the W L_3 -edge) [45]. Therefore, the lifetime broadening present in conventional XANES spectra is significantly reduced in the RXES experiment. As a result, additional features become visible in the HERFD-XANES spectra, which are blurred or poorly resolved with the traditional approach. A high-resolution spectrometer with the high brightness X-ray source and highly effective detectors are required to acquire them. At the same time, high penetration of hard X-ray radiation allows one to probe the sample bulk.

In the RXES experiment, the intensities and energies of the incoming and emitted X-rays are monitored. One way of presenting the RXES intensity plane is to plot the energy of emitted photons against the incident photon energy as shown in Fig. 3(a). Different plane cuts allow one to obtain valuable information on the structural and electronic properties of the material. For example, the W L_3 -edge HERFD-XANES spectrum can be obtained from Fig. 3(a) by integrating the emission intensity in the narrow emission energy region of ± 0.2 eV around 8398.5 eV. Thus extracted HERFD-XANES spectra of $\text{CuMo}_{1-x}\text{W}_x\text{O}_4$ solid solutions at 300 K are shown in Fig. 3(d).

Besides, the HERFD-XANES spectra, one can additionally obtain (Figs. 3(a,b)) high energy resolution off-resonant X-ray emission spectra by extracting them slightly below (bands B1 and B2 in Figs. 3(e,f)) and above (bands B3 and B4 in Figs. 3(g,h)) the W L_3 absorption edge, respectively. As one can see, both types of emission spectra contain information on the crystal field splitting, while with a smaller signal-to-noise ratio compared to

HERFD-XANES (Fig. 3(d)) due to weaker intensity. Besides, in the non-resonant case (Figs. 3(g,h)), the tails of the main X-ray emission line (W L_{α_1} in Fig. 3(b)) produce some background under the B3 and B4 bands, which also limits the accuracy of the analysis and should be removed in advance.

Further, we will discuss the effect of concentration and temperature on the local structure of tungsten ions in $\text{CuMo}_{1-x}\text{W}_x\text{O}_4$ solid solutions observed in the RXES spectra.

4.2. Effect of composition

The concentration dependences of the RXES spectra of $\text{CuMo}_{1-x}\text{W}_x\text{O}_4$ solid solutions at 300 K are shown in Figs. 3(d-h). The origin of the observed bands is due to three different mechanisms, already discussed above.

The emission spectra for the incident X-ray energy $E_i=10190$ eV below the W L_3 absorption edge are shown in Figs. 3(e,f) and correspond to off-resonant condition [46]. Two emission bands B1 at ~ 8312 eV and B2 at ~ 8376 eV can be distinguished in the spectra and correspond to the transitions from $3d_{3/2}$ and $3d_{5/2}$ levels, respectively (Figs. 3(b,c)). The intensity of the lower energy band B1 is smaller than that of the band B2, correlating with the intensity of the W L_{α_1} and L_{α_2} bands.

Both bands B1 and B2 are split into two peaks due to the crystal field of oxygen ligands. The distance between these peaks and the ratio I_1/I_2 of their intensities were evaluated by fitting the spectra with two Lorentzian functions and were used to estimate the symmetry of the crystal field. The difference between the position of the two Lorentzian functions is related to the crystal-field splitting parameter Δ or $10Dq$ used in the crystal-field theory [37].

One can see in Figs. 3(e,f), that the change of the spectral shape upon tungsten content increase indicates that the local coordination of tungsten ions changes from tetrahedral ($x = 0.04$) to octahedral ($x > 0.15$).

The emission spectra for the incident X-ray energy $E_i=10242$ eV well above the W L_3 absorption edge are reported in Figs. 3(g,h). In this case, four emission bands W $L\alpha_2$, B3, W $L\alpha_1$ and B4 are observed in Fig. 3(b). The origin of the bands B3 and B4 is similar to that of B1 and B2, i.e., is due to the transitions from $3d_{3/2}$ and $3d_{5/2}$ levels, respectively (Fig. 3(c)). Again the lower energy band B3 has a much weaker intensity than that of the band B4, and both bands are split by the crystal field to two peaks (Figs. 3(g,h)). Opposite to the case of the bands B1 and B2, the bands B3 and B4 are located on top of the background due to the W $L\alpha_1$ and partially W $L\alpha_2$ fluorescence, which makes it more difficult to determine the magnitude of the peaks splitting and the ratio of their intensities. Nevertheless, the obtained parameters agree well with that obtained from the analysis of the bands B1 and B2 suggesting the octahedral coordination of tungsten ions for $x > 0.15$.

Finally, the analysis was also performed for the W L_3 -edge HERFD-XANES spectra (Fig. 3(d)). Here the pronounced splitting of the white line due to the octahedral crystal field is clearly visible for $x > 0.15$ and agrees with the results obtained from X-ray fluorescence spectra in Figs. 3(e-h). The white line was fitted with two Lorentzian functions to estimate its splitting magnitude. The results for the crystal-field splitting parameter Δ obtained from the off-resonant XES and HERFD-XANES spectra of $\text{CuMo}_{1-x}\text{W}_x\text{O}_4$ solid solutions at 300 K and 90 K are combined in Fig. 4.

At 300 K, CuWO_4 ($x = 1$) and $\text{CuMo}_{0.96}\text{W}_{0.04}\text{O}_4$ ($x = 0.04$) have wol-

framite [35] and α -CuMoO₄ [34] phases, respectively, which correspond to the octahedral and tetrahedral coordination of tungsten ions. Upon cooling down to 90 K, CuWO₄ remains always in the triclinic phase (space group $P\bar{1}$) [47]. At the same time, CuMo_{0.96}W_{0.04}O₄ transforms on cooling to γ -CuMoO₄ phase [1, 2] with distorted octahedral coordination of Mo⁶⁺ and W⁶⁺ ions.

For intermediate compositions of CuMo_{1-x}W_xO₄ solid solutions, a mixture of α -CuMoO₄ and γ -CuMoO₄ phases co-exists in the samples with the relative amounts depending on the tungsten content and temperature range [1, 5, 48]. In particular, when samples are cooled from 300 K down to 90 K, a transition from tetrahedral-to-octahedral tungsten coordination is observed for $x < 0.20$ but not for $x \geq 0.20$ (Fig. 4).

Our theoretical XANES calculations for distorted WO₆ and WO₄ environments (Fig. 2) suggest a value of the parameter $\Delta \sim 3 - 4$ eV for octahedral coordination and about 2 eV for tetrahedral one. Therefore, taking into account the experimentally observed α -to- γ transition and theoretical predictions, two ranges of the crystal-field splitting parameter Δ can be identified (see green and brown regions in Fig. 4): the tetrahedral coordination of tungsten ions is expected for $\Delta < 3$, whereas the octahedral coordination for $\Delta > 3$. Thus, the simple analysis of the experimental off-resonant XES and HERFD-XANES spectra can provide useful information on the local coordination of tungsten ions. In the next section, we will demonstrate the sensitivity of the parameter Δ to the hysteretic phase transitions in CuMo_{1-x}W_xO₄.

Furthermore, we found that the parameter Δ correlates well with the solid

solution optical properties (their color). Namely, at 300 K, the samples with $x \leq 0.15$ have the crystal-field splitting parameter $\Delta < 3$ eV and greenish colour, whereas the samples with $x \geq 0.20$ have $\Delta > 3$ eV and brown colour. Note, that upon cooling of the samples with $x \leq 0.15$ down to 90 K, their color changes to brown, in agreement with previous studies [34], and the parameter Δ increases above 3 eV indicating the transition to the phase with the octahedral tungsten coordination.

4.3. Effect of temperature

It is known that the first-order structural phase transition between α and γ phases in $\text{CuMo}_{1-x}\text{W}_x\text{O}_4$ solid solutions for $x < 0.15$ has strong hysteretic behaviour, which can be controlled by the tungsten content [1, 5]. The hysteresis loop was first experimentally detected by optical, calorimetry and magnetic measurement [1].

In our previous studies [21, 49], we have shown for CuMoO_4 and $\text{CuMo}_{0.90}\text{W}_{0.10}\text{O}_4$ that the Mo K-edge XANES is sensitive to the α -to- γ phase transition due to the significant change in the local coordination of molybdenum ions from tetrahedral to octahedral one. Moreover, the analysis of the Mo K-edge XANES allowed us to determine the transition hysteresis loop and to estimate the fraction of α -phase upon cooling and heating. At the same time, the sensitivity of the Mo K-edge XANES to the α -to- γ transition is based on a variation of the pre-edge peak amplitude which is hidden by the natural broadening of the core level (5.8 eV at the Mo K-edge [24]). Therefore, the high resolution of the off-resonant XES and HERFD-XANES spectra (Fig. 3) should be more beneficial for tracking the α -to- γ phase transition.

An example of the temperature-dependent W L_3 -edge HERFD-XANES

spectra of $\text{CuMo}_{0.96}\text{W}_{0.04}\text{O}_4$ is shown in Fig. 5. The change of the spectral shape reflects a transition from tetrahedral (α -phase) to octahedral (γ -phase) tungsten coordination on cooling from 300 K to 120 K, whereas from octahedral to tetrahedral tungsten coordination on heating from 90 K to 420 K. Note that the effect is well observed in RXES planes as the temperature dependence of the relative position of two bright spots, which are well resolved in the octahedral coordination but change relative intensity and move closer in the tetrahedral one.

The phase transition hysteresis loops for $\text{CuMo}_{0.96}\text{W}_{0.04}\text{O}_4$ and $\text{CuMo}_{0.90}\text{W}_{0.10}\text{O}_4$ solid solutions are shown in Fig. 6. They were determined from the temperature dependencies of the magnitude of the peak splitting and the ratio I_1/I_2 of the peak intensities, which were obtained from the W L_3 -edge HERFD-XANES and off-resonant XES spectra normalized on a scale from 0 to 1 to display them on the same graph. Note that the two approaches have slightly different sensitivity to the change of tungsten coordination leading to some scatter of points. The results for $\text{CuMo}_{0.90}\text{W}_{0.10}\text{O}_4$ (Fig. 6(b)) are also compared with a fraction of the α -phase extracted from the analysis of the Mo K-edge XANES spectra reported in our previous work [21]. One can see a small difference between the starting temperatures of the α -to- γ phase transition obtained from the W L_3 and Mo K edges for $\text{CuMo}_{0.90}\text{W}_{0.10}\text{O}_4$ sample. When probed at the Mo K-edge, the transition starts at a slightly lower temperature than when measured at the W L_3 edge. This seeming contradiction has a simple explanation by the fact, that some part of the tungsten atoms is located in the octahedral environment already at room temperature, as was concluded above from Fig. 4.

5. Conclusions

Resonant X-ray emission spectroscopy at the W L₃-edge was used to study the changes in the local atomic structure of tungsten ions across the thermochromic phase transition in CuMo_{1-x}W_xO₄ solid solutions as a function of sample composition and temperature.

We demonstrated that the analysis of the RXES plane provides useful information on the coordination of tungsten atoms in the sample bulk and allows one to determine the crystal-field splitting parameter Δ for the 5d(W)-states. Moreover, this information can be extracted from the RXES plane using two different approaches by analysing the high-energy resolution fluorescence detected X-ray absorption near-edge structure (HERFD-XANES) and the high energy resolution off-resonant X-ray emission spectra excited below and above resonance conditions. The analysis of the RXES planes shows a clear advantage over conventional XANES due to revealing spectral features with much higher resolution.

The method is well suited for in-situ measurements and was used here to determine the hysteretic behaviour of the first-order structural phase transition between α and γ phases in CuMo_{1-x}W_xO₄ solid solutions on cooling and heating, even at low ($x < 0.10$) tungsten content.

We found that tungsten ions in CuMo_{1-x}W_xO₄ solid solutions have octahedral coordination for $x > 0.15$ at all temperatures, whereas their coordination changes from tetrahedral to octahedral upon cooling for smaller tungsten content. Nevertheless, some amount of tungsten ions co-exists in the octahedral environment at room temperature for $x < 0.15$. The obtained results correlate well with the optical properties of these materials, in partic-

ular, color change from green to brown upon cooling or increasing tungsten content.

The electronic structure of $\text{CuMo}_{1-x}\text{W}_x\text{O}_4$ solid solutions controls their thermochromic properties, which are related to a variation of the transmission window in optical spectra [1, 6]. A change in the local coordination of tungsten atoms from tetrahedral to octahedral affects the band gap, which is determined by the oxygen-to-metal charge transfer [1]. The band gap is smaller in the case of octahedral coordination of tungsten [6], i.e., at higher tungsten content or lower temperature.

To conclude, this study demonstrates the possibilities of the RXES technique to probe the crystal field effect in functional thermochromic materials with controllable properties on the example of $\text{CuMo}_{1-x}\text{W}_x\text{O}_4$ solid solutions.

Declaration of Competing Interest

The authors declare that they have no known competing financial interests or personal relationships that could have appeared to influence the work reported in this paper.

Acknowledgements

Financial support provided by Scientific Research Project for Students and Young Researchers Nr. SJZ/2019/1 realized at the Institute of Solid State Physics, University of Latvia is greatly acknowledged. The used infrastructure of the von Hamos spectrometer was realized in the frame of projects FKZ 05K13UK1 and FKZ 05K14PP1. The experiment at the PETRA III synchrotron was performed within the project No. I-20180615 EC.

The synchrotron experiments have been supported by the project CALIP-SOplus under the Grant Agreement 730872 from the EU Framework Programme for Research and Innovation HORIZON 2020. The experiment at the Elettra synchrotron was performed within the project No. 20150303. Institute of Solid State Physics, University of Latvia as the Center of Excellence has received funding from the European Union’s Horizon 2020 Framework Programme H2020-WIDESPREAD-01-2016-2017-TeamingPhase2 under grant agreement No. 739508, project CAMART2.

Supplementary materials

Supplementary material associated with this article can be found, in the online version, at doi: XXX.j.actamat.2020.YYY

References

- [1] M. Gaudon, C. Carbonera, A. E. Thiry, A. Demourgues, P. Deniard, C. Payen, J. F. Létard, S. Jobic, Adaptable thermochromism in the $\text{CuMo}_{1-x}\text{W}_x\text{O}_4$ series ($0 \leq x < 0.1$): a behavior related to a first-order phase transition with a transition temperature depending on x , *Inorg. Chem.* 46 (2007) 10200–10207. doi:10.1021/ic701263c.
- [2] M. Gaudon, P. Deniard, A. Demourgues, A. E. Thiry, C. Carbonera, A. Le Nestour, A. Largeau, J. F. Létard, S. Jobic, Unprecedented “one-finger-push”-induced phase transition with a drastic color change in an inorganic material, *Adv. Mater.* 19 (2007) 3517–3519. doi:10.1002/adma.200700905.

- [3] M. Gaudon, B. Basly, Y. Fauque, J. Majimel, M. H. Delville, Thermochromic phase transition on $\text{CuMo}_{0.9}\text{W}_{0.1}\text{O}_4@\text{SiO}_2$ core-shell particles, *Inorg. Chem.* 48 (2009) 2136–2139. doi:10.1021/ic802057c.
- [4] I. Yanase, T. Mizuno, H. Kobayashi, Structural phase transition and thermochromic behavior of synthesized W-substituted CuMoO_4 , *Ceram. Int.* 39 (2013) 2059–2064. doi:10.1016/j.ceramint.2012.08.059.
- [5] L. Robertson, N. Penin, V. Blanco-Gutierrez, D. Sheptyakov, A. Demourgues, M. Gaudon, $\text{CuMo}_{0.9}\text{W}_{0.1}\text{O}_4$ phase transition with thermochromic, piezochromic, and thermosalient effects, *J. Mater. Chem. C* 3 (2015) 2918–2924. doi:10.1039/C4TC02463J.
- [6] X. Wu, C. Fu, J. Cao, C. Gu, W. Liu, Effect of W doping on phase transition behavior and dielectric relaxation of CuMoO_4 obtained by a modified sol-gel method, *Mater. Res. Express* 7 (2020) 016309. doi:10.1088/2053-1591/ab6546.
- [7] V. Blanco-Gutierrez, L. Cornu, A. Demourgues, M. Gaudon, $\text{CoMoO}_4/\text{CuMo}_{0.9}\text{W}_{0.1}\text{O}_4$ mixture as an efficient piezochromic sensor to detect temperature/pressure shock parameters, *ACS Appl. Mater. Interfaces* 7 (2015) 7112–7117. doi:10.1021/am508652h.
- [8] M. Gaudon, C. Riml, A. Turpain, C. Labrugere, M. H. Delville, Investigation of the chromic phase transition of $\text{CuMo}_{0.9}\text{W}_{0.1}\text{O}_4$ induced by surface protonation, *Chem. Mater.* 22 (2010) 5905–5911. doi:10.1021/cm101824d.

- [9] J. C. Hill, Y. Ping, G. A. Galli, K.-S. Choi, Synthesis, photoelectrochemical properties, and first principles study of n-type $\text{CuW}_{1-x}\text{Mo}_x\text{O}_4$ electrodes showing enhanced visible light absorption, *Energy Environ. Sci.* 6 (2013) 2440–2446. doi:10.1039/C3EE40827B.
- [10] Q. Liang, Y. Guo, N. Zhang, Q. Qian, Y. Hu, J. Hu, Z. Li, Z. Zou, Improved water-splitting performances of $\text{CuW}_{1-x}\text{Mo}_x\text{O}_4$ photoanodes synthesized by spray pyrolysis, *Sci. China Mater.* 61 (2018) 1297–1304. doi:10.1007/s40843-018-9287-5.
- [11] N. Joseph, J. Varghese, M. Teirikangas, H. Jantunen, A temperature-responsive copper molybdate polymorph mixture near to water boiling point by a simple cryogenic quenching route, *ACS Appl. Mater. Interfaces* 12 (2020) 1046–1053. doi:10.1021/acsami.9b17300.
- [12] G. Steiner, R. Salzer, W. Reichelt, Temperature dependence of the optical properties of CuMoO_4 , *Fresenius J. Anal. Chem.* 370 (2001) 731–734. doi:10.1007/s002160000630.
- [13] I. Jonane, A. Anspoks, G. Aquilanti, A. Kuzmin, High-temperature X-ray absorption spectroscopy study of thermochromic copper molybdate, *Acta Mater.* 179 (2019) 26–35. doi:10.1016/j.actamat.2019.06.034.
- [14] S. Bordiga, E. Groppo, G. Agostini, J. A. van Bokhoven, C. Lamberti, Reactivity of surface species in heterogeneous catalysts probed by In situ X-ray absorption techniques, *Chem. Rev.* 113 (2013) 1736–1850. doi:10.1021/cr2000898.

- [15] N. A. Young, The application of synchrotron radiation and in particular X-ray absorption spectroscopy to matrix isolated species, *Coord. Chem. Rev.* 277-278 (2014) 224–274. doi:10.1016/j.ccr.2014.05.010.
- [16] V. R. Mastelaro, E. D. Zanotto, X-ray absorption fine structure (XAFS) studies of oxide glasses-A 45-year overview, *Materials* 11 (2018) 204. doi:10.3390/ma11020204.
- [17] J. Timoshenko, A. Anspoks, A. Kalinko, I. Jonane, A. Kuzmin, Local structure of multiferroic MnWO_4 and $\text{Mn}_{0.7}\text{Co}_{0.3}\text{WO}_4$ revealed by the evolutionary algorithm, *Ferroelectrics* 483 (2015) 68–74. doi:10.1080/00150193.2015.1058687.
- [18] A. Kalinko, M. Bauer, J. Timoshenko, A. Kuzmin, Molecular dynamics and reverse Monte Carlo modeling of scheelite-type AWO_4 (A= Ca, Sr, Ba) W L_3 -edge EXAFS spectra, *Phys. Scr.* 91 (2016) 114001. doi:10.1088/0031-8949/91/11/114001.
- [19] J. Timoshenko, A. Anspoks, A. Kalinko, A. Kuzmin, Local structure of cobalt tungstate revealed by EXAFS spectroscopy and reverse Monte Carlo/evolutionary algorithm simulations, *Z. Phys. Chem.* 230 (2016) 551–568. doi:10.1515/zpch-2015-0646.
- [20] A. Kuzmin, J. Timoshenko, A. Kalinko, I. Jonane, A. Anspoks, Treatment of disorder effects in X-ray absorption spectra beyond the conventional approach, *Rad. Phys. Chem.* 175 (2020) 108112. doi:10.1016/j.radphyschem.2018.12.032.

- [21] I. Jonane, A. Cintins, A. Kalinko, R. Chernikov, A. Kuzmin, Low temperature X-ray absorption spectroscopy study of CuMoO_4 and $\text{CuMo}_{0.90}\text{W}_{0.10}\text{O}_4$ using reverse Monte-Carlo method, *Rad. Phys. Chem.* 175 (2020) 108411.
- [22] S. Yamazoe, Y. Hitomi, T. Shishido, T. Tanaka, XAFS study of tungsten L_1 - and L_3 -edges: structural analysis of WO_3 species loaded on TiO_2 as a catalyst for photo-oxidation of NH_3 , *J. Phys. Chem. C* 112 (2008) 6869–6879. doi:10.1021/jp711250f.
- [23] U. Jayarathne, P. Chandrasekaran, A. F. Greene, J. T. Mague, S. DeBeer, K. M. Lancaster, S. Sproules, J. P. Donahue, X-ray absorption spectroscopy systematics at the tungsten L-edge, *Inorg. Chem.* 53 (2014) 8230–8241. doi:10.1021/ic500256a.
- [24] O. Keski-Rahkonen, M. O. Krause, Total and partial atomic-level widths, *At. Data Nucl. Data Tables* 14 (1974) 139–146. doi:10.1016/S0092-640X(74)80020-3.
- [25] A. Balerna, E. Bernieri, E. Burattini, A. Kuzmin, A. Lusic, J. Purans, P. Cikmach, XANES studies of MeO_{3-x} ($\text{Me} = \text{W}, \text{Re}, \text{Ir}$) crystalline and amorphous oxides, *Nucl. Instrum. Methods Phys. Res. A* 308 (1991) 240–242. doi:10.1016/0168-9002(91)90637-6.
- [26] A. Kuzmin, J. Purans, X-ray absorption spectroscopy study of the local environment around tungsten and molybdenum ions in tungsten-phosphate and molybdenum-phosphate glasses, *Proc. SPIE* 2968 (1997) 180–185. doi:10.1117/12.266831.

- [27] P. Charton, L. Gengembre, P. Armand, TeO₂-WO₃ glasses: infrared, XPS and XANES structural characterizations, *J. Solid State Chem.* 168 (2002) 175–183. doi:10.1006/jssc.2002.9707.
- [28] W. A. Caliebe, V. Murzin, A. Kalinko, M. Görlitz, High-flux XAFS-beamline P64 at PETRA III, *AIP Conf. Proc.* 2054 (2019) 060031. doi:10.1063/1.5084662.
- [29] A. Kalinko, W. A. Caliebe, R. Schoch, M. Bauer, A von Hamos-type hard X-ray spectrometer at the PETRA III beamline P64, *J. Synchrotron Rad.* 27 (2020) 31–36. doi:10.1107/S1600577519013638.
- [30] A. Di Cicco, G. Aquilanti, M. Minicucci, E. Principi, N. Novello, A. Cognigni, L. Olivi, Novel XAFS capabilities at ELETTRA synchrotron light source, *J. Phys.: Conf. Ser.* 190 (2009) 012043. doi:10.1088/1742-6596/190/1/012043.
- [31] Y. Joly, X-ray absorption near-edge structure calculations beyond the muffin-tin approximation, *Phys. Rev. B* 63 (2001) 125120. doi:10.1103/PhysRevB.63.125120.
- [32] O. Bunău, Y. Joly, Self-consistent aspects of x-ray absorption calculations, *J. Phys.: Condens. Matter* 21 (2009) 345501. doi:10.1088/0953-8984/21/34/345501.
- [33] L. Hedin, B. I. Lundqvist, Explicit local exchange-correlation potentials, *J. Phys. C: Solid State Phys.* 4 (1971) 2064–2083. doi:10.1088/0022-3719/4/14/022.

- [34] M. Wiesmann, H. Ehrenberg, G. Miehe, T. Peun, H. Weitzel, H. Fuess, *p-T* phase diagram of CuMoO_4 , *J. Solid State Chem.* 132 (1997) 88–97. doi:10.1006/jssc.1997.7413.
- [35] J. Forsyth, C. Wilkinson, A. Zvyagin, The antiferromagnetic structure of copper tungstate, CuWO_4 , *J. Phys.: Condens. Matter* 3 (1991) 8433. doi:10.1088/0953-8984/3/43/010.
- [36] R. D. Shannon, Revised effective ionic radii and systematic studies of interatomic distances in halides and chalcogenides, *Acta Cryst. A* 32 (1976) 751–767. doi:10.1107/S0567739476001551.
- [37] I. B. Bersuker, *Electronic Structure and Properties of Transition Metal Compounds: Introduction to the Theory*, 2nd Edition, John Wiley & Sons, Hoboken, New Jersey, 2010. doi:10.1002/9780470573051.
- [38] M. Brown, R. E. Peierls, E. A. Stern, White lines in x-ray absorption, *Phys. Rev. B* 15 (1977) 738–744. doi:10.1103/PhysRevB.15.738.
- [39] H. A. Kramers, W. Heisenberg, Über die streuung von strahlung durch atome, *Z. Physik* 31 (1925) 681–708. doi:10.1007/BF02980624.
- [40] P. Glatzel, U. Bergmann, High resolution 1s core hole X-ray spectroscopy in 3d transition metal complexes – electronic and structural information, *Coord. Chem. Rev.* 249 (2005) 65–95. doi:10.1016/j.ccr.2004.04.011.
- [41] J.-P. Rueff, A. Shukla, Inelastic x-ray scattering by electronic excitations under high pressure, *Rev. Mod. Phys.* 82 (2010) 847–896. doi:10.1103/RevModPhys.82.847.

- [42] P. Glatzel, M. Sikora, G. Smolentsev, M. Fernández-García, Hard X-ray photon-in photon-out spectroscopy, *Catal. Today* 145 (2009) 294–299. doi:10.1016/j.cattod.2008.10.049.
- [43] J.-P. Rueff, A. Shukla, A RIXS cookbook: Five recipes for successful RIXS applications, *J. Electron Spectrosc. Relat. Phenom.* 188 (2013) 10–16. doi:10.1016/j.elspec.2013.04.014.
- [44] M. Rovezzi, P. Glatzel, Hard x-ray emission spectroscopy: a powerful tool for the characterization of magnetic semiconductors, *Semicond. Sci. Technol.* 29 (2) (2014) 023002. doi:10.1088/0268-1242/29/2/023002.
- [45] A. Wach, J. Sá, J. Szlachetko, Comparative study of the around-Fermi electronic structure of $5d$ metals and metal-oxides by means of high-resolution X-ray emission and absorption spectroscopies, *J. Synchrotron Rad.* 27 (2020) 689–694. doi:10.1107/S1600577520003690.
- [46] W. Błachucki, J. Hozowska, J.-C. Dousse, Y. Kayser, R. Stachura, K. Tyrała, K. Wojtaszek, J. Sá, J. Szlachetko, High energy resolution off-resonant spectroscopy: A review, *Spectrochimica Acta B* 136 (2017) 23–33. doi:10.1016/j.sab.2017.08.002.
- [47] von Hans Weitzel, Magnetische struktur von CoWO_4 , NiWO_4 und CuWO_4 , *Solid State Commun.* 8 (1970) 2071–2072. doi:10.1016/0038-1098(70)90221-8.
- [48] M. Benchikhi, R. El Ouati, S. Guillemet-Fritsch, L. Er-Rakho, B. Durand, Investigation of structural transition in molybdates

$\text{CuMo}_{1-x}\text{W}_x\text{O}_4$ prepared by polymeric precursor method, *Process. Appl. Ceram.* 11 (2017) 21–26. doi:10.2298/PAC1701021B.

- [49] I. Jonane, A. Cintins, A. Kalinko, R. Chernikov, A. Kuzmin, X-ray absorption near edge spectroscopy of thermochromic phase transition in CuMoO_4 , *Low Temp. Phys.* 44 (2018) 434–437. doi:10.1063/1.5034155.

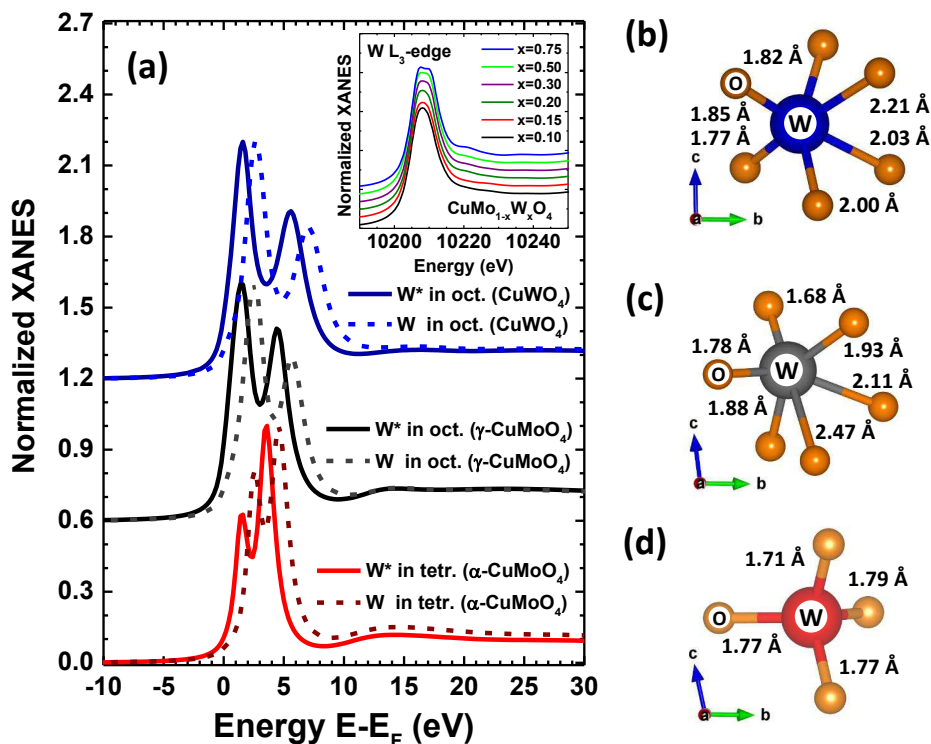


Figure 2: (a) Calculated W L_3 -edge XANES spectra for tungsten atoms in distorted octahedral (CuWO_4 and W substituting molybdenum atoms at the Mo2 site in $\gamma\text{-CuMoO}_4$) and tetrahedral (W substituting molybdenum atoms at the Mo2 site in $\alpha\text{-CuMoO}_4$) environments. The results for the excited state with the core hole (W^* , solid curves) and non-excited state without the core hole (W, dashed curves) are given. Tungsten–oxygen polyhedra with indicated interatomic distances in (b) CuWO_4 , (c) W at the Mo2 site in $\gamma\text{-CuMoO}_4$ and (d) W at the Mo2 site in $\alpha\text{-CuMoO}_4$ are also shown. Inset shows the experimental W L_3 -edge XANES spectra in $\text{CuMo}_{1-x}\text{W}_x\text{O}_4$ solid solutions measured in the transmission mode.

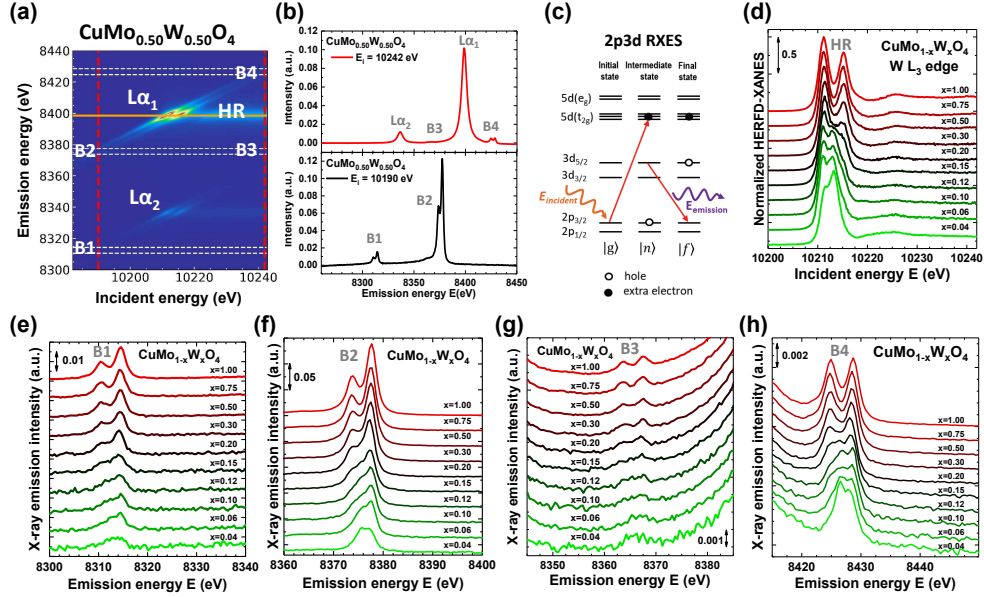


Figure 3: (a) RXES intensity map as a function of incident and emitted energies for $\text{CuMo}_{0.50}\text{W}_{0.50}\text{O}_4$ solid solution at 300 K. (b) Vertical cuts of the RXES plane at the incident energies $E_i=10190$ eV and 10242 eV, shown in (a) by two vertical red dashed lines. Principal observed bands ($L\alpha_1, \alpha_2$ and B1-B4) are labeled. (c) A schematic diagram of 2p3d RXES process for octahedral tungsten coordination showing initial, intermediate and final states. (d) The W L_3 -edge HERFD-XANES spectra for different $\text{CuMo}_{1-x}\text{W}_x\text{O}_4$ solid solutions measured at the emission energy $E_e=8398.5\pm 0.2$ eV, indicated by the horizontal orange solid line in (a). (e,f) High energy resolution off-resonant X-ray spectra for different $\text{CuMo}_{1-x}\text{W}_x\text{O}_4$ solid solutions obtained at $E_i=10190$ eV below the W L_3 -edge. (g,h) High energy resolution off-resonant X-ray emission spectra for different $\text{CuMo}_{1-x}\text{W}_x\text{O}_4$ solid solutions obtained at $E_i=10242$ eV above the W L_3 -edge.

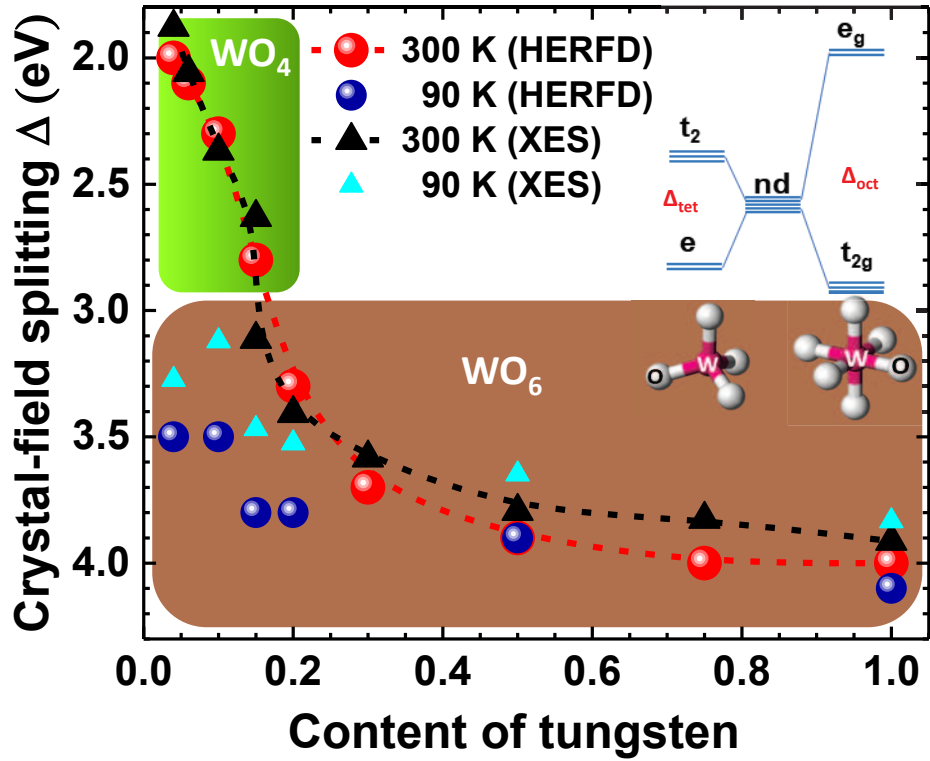


Figure 4: Crystal-field splitting parameter Δ as a function of tungsten content x in $\text{CuMo}_{1-x}\text{W}_x\text{O}_4$ solid solutions at 90 K and 300 K calculated from off-resonant XES (Fig. 3(f)) and HERFD-XANES (Fig. 3(d)) spectra. Schematic energy level diagram showing crystal-field splitting of tungsten 5d-states in the tetrahedral and octahedral environment is also shown. Note that Δ_{tet} is smaller than Δ_{oct} .

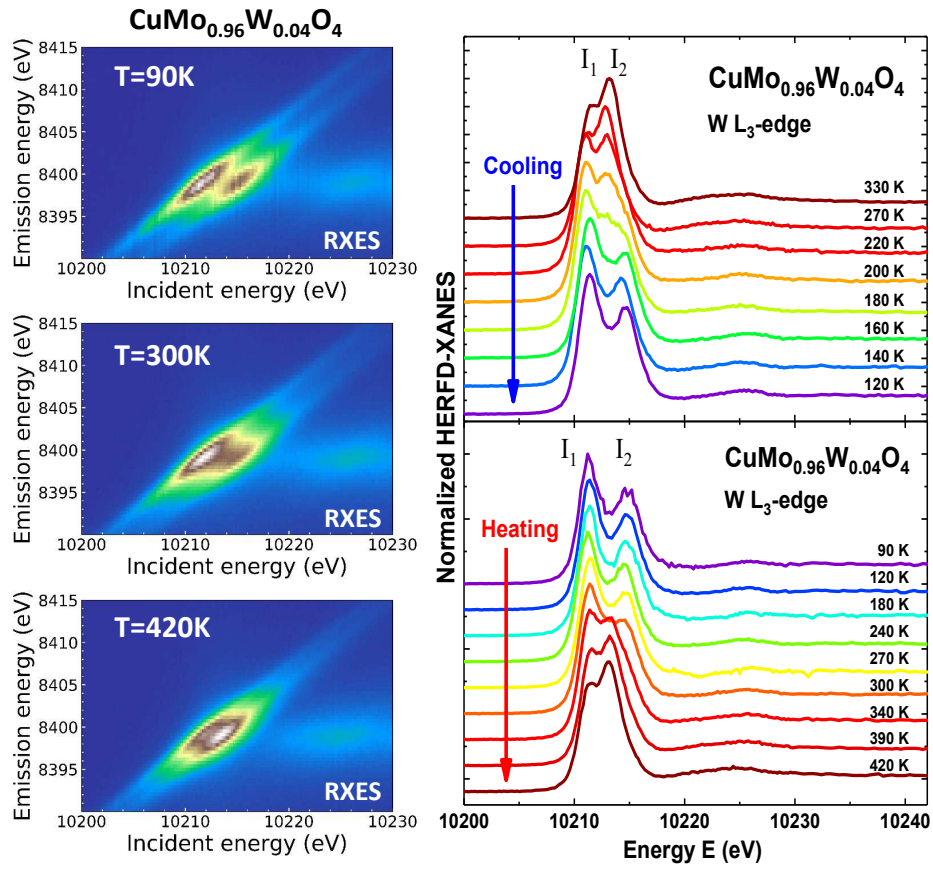


Figure 5: Parts of the RXES planes at 90 K, 300 K and 420 K on heating (left panels) and temperature dependent W L₃-edge HERFD-XANES spectra measured on cooling and heating (right panel) for CuMo_{0.96}W_{0.04}O₄.

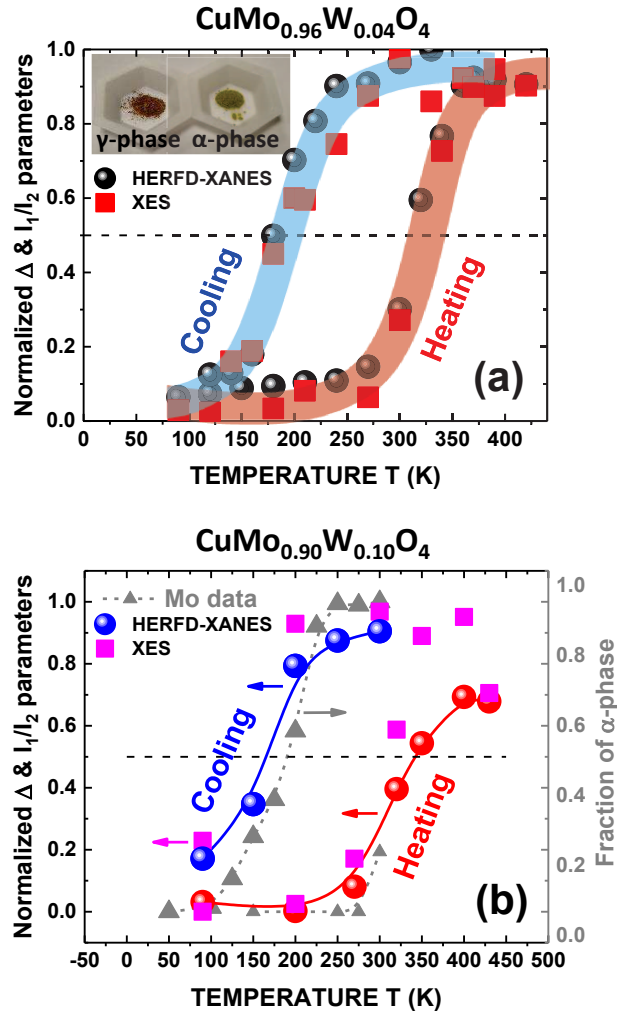


Figure 6: Temperature dependencies of the magnitude of the peak splitting (Δ) and the ratio of the white line peak intensities (I_1/I_2) for $\text{CuMo}_{0.96}\text{W}_{0.04}\text{O}_4$ (a) and $\text{CuMo}_{0.90}\text{W}_{0.10}\text{O}_4$ (b). A fraction of the α -phase extracted from the analysis of the Mo K-edge XANES spectra of $\text{CuMo}_{0.90}\text{W}_{0.10}\text{O}_4$ [21] is also displayed for comparison (solid triangles). Inset shows a photo of two $\text{CuMo}_{0.96}\text{W}_{0.04}\text{O}_4$ samples at room temperature: the brown sample is in the γ -phase (after treatment at 77 K in liquid nitrogen), and the green sample is in the α -phase.